Biased resistor network model for electromigration failure and related phenomena in metallic lines

C. Pennetta,[1,2,*] E. Alfinito,[1,2] L. Reggiani,[1,2] F. Fantini,[3] I. DeMunari,[4] and A. Scorzoni[5]
[1]*INFM—National Nanotechnology Laboratory, Via Arnesano, I-73100, Lecce, Italy*
[2]*Dipartimento di Ingegneria dell'Innovazione, Università di Lecce, Italy*
[3]*INFM and Dipartimento di Ingegneria dell'Informazione, Università di Modena, Via Vignolese 905, I-41100 Modena, Italy*
[4]*INFM and Dipartimento di Ingegneria dell'Informazione, Università di Parma, Parco Area delle Scienze 181/A, I-43100 Parma, Italy*
[5]*INFN and Dipartimento di Ingegneria Elettronica e dell'Informazione, Università di Perugia, Via G. Duranti 93, I-06125 Perugia, Italy*

(Received 24 February 2004; revised manuscript received 11 May 2004; published 19 November 2004)

Electromigration phenomena in metallic lines are studied by using a biased resistor network model. The void formation induced by the electron wind is simulated by a stochastic process of resistor breaking, while the growth of mechanical stress inside the line is described by an antagonist process of recovery of the broken resistors. The model accounts for the existence of temperature gradients due to current crowding and Joule heating. Alloying effects are also accounted for. Monte Carlo simulations allow the study within a unified theoretical framework of a variety of relevant features related to the electromigration. The predictions of the model are in excellent agreement with the experiments and in particular with the degradation towards electrical breakdown of stressed Al–Cu thin metallic lines. Detailed investigations refer to the damage pattern, the distribution of the times to failure (TTFs), the generalized Black's law, the time evolution of the resistance, including the early-stage change due to alloying effects and the electromigration saturation appearing at low current densities or for short line lengths. The dependence of the TTFs on the length and width of the metallic line is also well reproduced. Finally, the model successfully describes the resistance noise properties under steady state conditions.

DOI: 10.1103/PhysRevB.70.174305 PACS number(s): 66.30.Qa, 85.40.Qx, 85.40.Ls, 64.60.Ak

I. INTRODUCTION

The phenomenon of electromigration (EM) is typical of metallic conductors and consists of a nonsteady atomic transport driven by electronic currents of high density.[1,2] The nonsteady atomic transport gives rise to the formation and growth of voids and hillocks in different regions of the conductor (EM damage).[1,2] This damage cumulates progressively and, when the current is applied for a sufficiently long time, a void grows enough to break completely the metallic line, implying an irreversible failure process. The time required for this process defines the time to failure (TTF) of the metallic line[1,2] (though alternative failure criteria can be found in the literature[1–3]). The importance of EM is largely due to the fact that it is the most common mechanism of failure of the metallic interconnects present in any electronic device.[1–3] As a consequence, a huge number of experimental[4–16] and theoretical[17–25] studies have been and are yet devoted to the subject, especially in the context of modern nanoelectronics.

The central issue in EM degradation phenomena is the determination of the TTF and its statistical properties.[1–3] TTFs are measured under very high stress conditions (currents and temperature much higher than those corresponding to the usual operating conditions of the devices) in the so called accelerated tests.[1,2] The extrapolation to normal operating conditions is generally performed on the basis of three frequently adopted assumptions.[1,2] First, TTFs are taken to follow a lognormal distribution (which means that the logarithms of TTFs are normally distributed). This distribution is then characterized by two parameters: the median time to failure, t_{50}, and the shape factor, s, where t_{50} is the time corresponding to the failure of 50% of the lines in the statistical sample and s is the lognormal root-mean-square deviation.[1] This distribution has been observed in many EM failure tests[1–3,7,8,14] and, recently, new testing techniques[14] allowing the analysis of very large statistical samples, have shown that the TTF distribution follows a perfect lognormal behavior down to four shape factors.[14] In spite of this evidence, no satisfactory eplanation has been given until now for the lognormality of the TTF distribution.[1,2,18]

The second assumption concerns the independence of the distribution shape factor of the stress conditions. Actually, s was found to be independent of temperature in all the range of values usually considered in accelerated tests.[1–3,7,8,14] On the contrary, a broadening of the distribution has been observed at the lowest current densities used in these tests.[3,7,8] This broadening of the distribution at low stress conditions has crucial implications on the evaluation of the minimum time to failure, i.e., the time corresponding to the first failure of a line of the family.[7,8] We will discuss this point in Sec. III B together with the results of our simulations.

The third assumption concerns the validity of the following empirical law, known as Black's law,[1,2,26] relating t_{50} to the current density, j, and temperature, T:

$$t_{50} = Cj^{-n} \exp\left[\frac{E}{k_B T}\right], \tag{1}$$

where C is a fitting amplitude, n the so called current exponent, E the EM activation energy and k_B the Boltzmann con-

stant. The validity of this law is confirmed by many experiments.[1–3] However, the simple power law behavior described by Eq. (1), generally holds in a limited range of intermediate current densities.[1–3] At high current densities, another power law with a different (higher) exponent is frequently observed and usually attributed to Joule heating effects,[1–3,23] while at low current densities t_{50} deviates from a power law, showing a tendency to diverge.[2,7] Furthermore, even in the intermediate range of j values, there is no agreement in the literature about the value of the current exponent.[1–3,17,23] We will come back on this subject in Sec. III B, discussing our results.

The geometry of the line plays a crucial role on the EM damage.[1–3,9,27] In fact, the depletion and accumulation of mass in different regions of the film, under the driving force exerted by the electronic current, determines the growth of mechanical stress gradients. The last ones give rise to an atomic back-flow which contrasts the EM process.[1,2,27] As the strength of these gradients depends strongly on the line geometry,[1,2,9,27] geometrical parameters have a fundamental role in the occurrence of failures. In particular, the competition between the driving force of the electronic current and the action of mechanical stress gradients, results in the existence of a current density threshold below which EM is stopped.[27] This condition was expressed by Blech and Herring[27] in the following equation which relates the threshold current density with the length of the line:

$$(jL)_c = \frac{(\Omega_a \Delta\sigma)}{(\rho Z^* e)}, \tag{2}$$

where Ω_a is the atomic volume, $\Delta\sigma$ is the maximum value of the mechanical stress difference between the line terminals that a line of length L can bear, ρ is the resistivity of the line, e the electronic charge and Z^* an average effective charge.[1,2,27] Equation (2), known as Blech's law,[27] defines the so called threshold product, $(jL)_c$. We will discuss the role of the line geometry on the EM failure process in Sec. III C.

Another fundamental ingredient in the understanding of the EM damage of interconnects is represented by the granular structure of the materials employed, Al, Cu, Ag, Al alloys, etc.[1–3] Furthermore, it must be noted that a high degree of disorder is usually present in alloy films (typically Al−Cu, Al−Si) due to alloying effects[2,10,11,28–30] and to thermal gradients.[1,2]

A large number of models has been proposed for the study of EM.[17–25] Many of them are microscopic models which address the problem of identifying the mechanisms responsible for the degradation process in terms of the peculiarities of the material considered.[19,21,22,24,25] Then, by using appropriate kinetic equations, some specific features of the damage process are determined and compared with experiments.[19,21,22,24,25] If the peculiarities of the material are sufficiently well accounted for, the predictivity of these models is very high[19,21,25] and therefore they can be very useful for applicative purposes. However, the approach used by many of these models intrinsically limits their predictivity to some specific features of the EM damage.

Another class of EM models has also been developed in the literature,[20,28] based on a "coarse grain" random resistor network (RN) approach.[31–34] Actually, the use of this kind of model is particularly appropriate in consequence of the granular structure of the materials used for the interconnects. Indeed, it has been observed that the atomic transport through grain boundaries and interfaces (transport channels) far exceeds that through the bulk of the grains.[1,2] Therefore, it is generally possible to neglect mass transport everywhere except within these channels and to describe the film as an interconnected network of atomic conducting paths.[1]

Bradley *et al.*[20] were the first to propose and apply to the study of EM a kinetic version of the random fuse model.[35] The dynamic fuse model introduced by these authors[20] adopts a failure criterion for the elementary resistor of the network suitable for the description of the EM process. The predictions of this model concerning the damage pattern and TTFs (maximum and minimum TTF, relationship of the median time to failure with the current, the temperature and the line geometry) shows the effectiveness and the potentiality of the resistor network approach.[20] However, the model of Bradley *et al.* cannot describe many other features of EM. In fact this model, though giving a good description of the driving force of the electronic current, does not take into account the antagonist action exerted by mechanical stress gradients. On the other hand, the competition between these two effects is essential for giving rise to a threshold current for EM.[1,2] Therefore, all the phenomenology related to the Blech's law[1,2,9,27] and saturation effects[9] cannot be accounted for within Bradley's model. Moreover, this model completely neglects Joule heating effects which are present in the high stress condition.[1,2]

Here, we illustrate a theoretical approach to EM which aims at studying the different features associated with this phenomenon within a unified theoretical framework. Similarly to the approach of Bradley *et al.*, our study is performed by renouncing to provide a description of the kinetics at an atomistic level and by adopting the RN approach, thus focusing on the correlations established by the electronic current among the different components of the system (grains, clusters of grains, interfaces, etc., i.e. atomic transport channels). However, in contrast to the dynamic fuse model,[20] we use the biased percolation model,[36,37] which adopts a probabilistic failure criterion for the elementary resistor of the network. The EM damage is described in terms of competition between two biased stochastic processes taking place in a resistor network.[28] Then, by means of Monte Carlo (MC) simulations, we are able to study a variety of relevant features of EM degradation. Early stage results have been presented in Refs. 28 and 38. In this article, we present a comprehensive study which includes many fundamental new features.

As a first we will show results concerning the damage pattern, the resistance evolution and alloying effects. Then, large attention will be devoted to the behavior of TTFs. We will show that the model correctly predicts a lognormal distribution for them, perfectly superimposing with the experimental one. The dependence of the parameters of the TTF distribution on temperature and current has also been investigated. Black's law[1,2,26] has been recovered not only for low

but also for high current values and the current exponents are in good agreement with the experimental results in both cases. By using a rectangular geometry, the dependence of TTFs on the length and width of the metallic line has been investigated, so that, for a fixed width, Blech's law[1,2,27] has been tested and a general expression has been obtained for the dependence of TTFs on both length and width. Finally, but not of minor interest, we have considered resistance saturation effects[9] and the properties of resistance fluctuations, by focusing on the non-Gaussianity of the distribution and on their power spectrum. Thus, our approach is able to account for a phenomenological scenario much wider than that considered by all existing EM models.

Finally, we emphasize the fact that the interest in EM phenomena is not limited to strictly applicative and practical purposes. Indeed, the understanding of nonequilibrium and failure phenomena in disordered systems represents a fundamental topic which has attracted a large attention in the recent literature.[31–37,39–46] In this respect, it must be noted that EM, which occurs in granular materials, in the presence of a significant disorder, driven by an external bias and contrasted by growth of mechanical stress gradients, exhibits practically all the main ingredients to represents a paradigmatic example of a failure process in a disordered system.

The paper is organized as follows. In Sec. II we briefly survey the theoretical model and define the parameters of interest. In Sec. III we present the results in connection with (A) resistance evolution, (B) stress conditions, (C) geometrical effects, (D) resistance saturation and fluctuations. In Sec. IV we draw the main conclusions.

II. MODEL

We describe a thin metallic line of length L, width W and thickness t_h as a two-dimensional resistor network of rectangular shape and square-lattice structure. The network of resistance R is made by N_L and N_W resistors in the length and width directions, respectively. The external bias, represented by a constant voltage V or a constant current I, is applied to the RN through electrical contacts realized by perfectly conducting bars at the left and right hand sides of the network. Thus, the total number of network resistors (excluding the contacts) is $N_{tot}=2N_LN_W+N_L-N_W$. Each resistor can be associated with a single grain, a small cluster of grains or an interfacial path. By denoting with d the average size of the grains, of the grain clusters or of the interfacial path, the values of N_L and N_W can be related to the ratios L/d and W/d, respectively. The network lies on an insulating substrate at temperature T_0, acting as a thermal bath, and it is made by three kinds of resistors: (i) regular resistors, (ii) impurity resistors, (iii) broken resistors. The regular resistors are associated with grains of "normal" resistivity (void free). The resistance of these resistors depends linearly on temperature, according to the expression

$$r_{reg,n}(T_n) = r_{ref}[1 + \alpha(T_n - T_{ref})], \tag{3}$$

where n is the resistor label, α the temperature coefficient of the resistance (TCR), T_n the local temperature, T_{ref} and r_{ref} the reference values for the TCR. When the Joule heating is negligible $T_n=T_0$ and the regular resistors are all equal to $r_0 \equiv r_{reg}(T_0)$. The impurity resistors of resistance $r_{imp}<r_0$ are associated with the formation/dissolution of $CuAl_2$ precipitates (low-resistivity cluster) during the stress conditions. Thus, they account for the variation in the alloy composition during the EM test due to the electron wind and/or to thermal effects (alloying effects).[11,28–30] Finally, the broken resistors correspond to the presence of microvoids at the grain boundary and, possibly, inside the grains. These broken resistors of resistance r_{OP} (OP stays for open circuit) are thus associated with very high resistivity regions inside the line. Here, we have taken $r_{OP}=10^9 r_0$. The existence of temperature gradients due to current crowding and Joule heating effects is accounted for by taking the local temperature of the n-th resistor (regular, impurity or broken) of resistance r_n given by the following expression:[37]

$$T_n = T_0 + A\left[r_n i_n^2 + \frac{B}{N_{neig}} \sum_{m=1}^{N_{neig}} (r_{m,n} i_{m,n}^2 - r_n i_n^2) \right], \tag{4}$$

where A is the thermal resistance of the single resistor, N_{neig} is the number of first neighbors of the n-th resistor, i_n the current flowing in it and $i_{m,n}$ is the current flowing in the m-th neighbor. The value $B=3/4$ is chosen to provide uniform heating of the perfect network, i.e. made by identical resistors. Equation (4) is the Fourier equation written by taking the simplifying assumption of instantaneous thermalization of the resistor, i.e. by taking a stationary regime and neglecting time dependent effects in the heat diffusion.[47] Under this hypothesis, the diffusive term must balance the term related to the power supplied by the external current and generated on the resistor or transmitted to it by mutual interactions. A simplified form of Eq. (4), not including thermal exchanges with neighbor resistors, has been first proposed by Gingl *et al.*[36] For a perfect[48] or nearly perfect network of resistance R_0, when a mean-field approach is meaningful, the average temperature increase is thus[49]

$$\Delta T = AR_0 I^2 / N_{tot} \equiv \theta R_0 I^2, \tag{5}$$

where $\theta=A/N_{tot}$ is the structure thermal resistance.[1,2]

The EM damage, consisting of the formation of microvoids under the action of the electron wind, is simulated by a stochastic process of resistor breaking. In other terms, we consider that the transformation of the n-th resistor (regular or impurity) into a broken one, $r_n \rightarrow r_{OP}$, can occur with probability $W_{OP,n}$. By adopting the biased percolation model,[36,37] we have taken the following expression for $W_{OP,n}$:

$$W_{OP,n} = \exp[-E_{OP}/k_B T_n], \tag{6}$$

where E_{OP} is a characteristic activation energy. In fact, Eq. (6) coupled with Eq. (4) implies that the void formation process is a biased percolation.[36,37] This means a probability of breaking a resistor (generation of microvoids) higher for resistors crossed by high current values.[36,37] Thus, the breaking probability is nonuniform for the different resistors in the network and it changes with time. We note that $W_{OP,n}$ depends on the current distribution, which in turn depends on the network configuration.[36,37] As the last one results from a

progressive accumulation of damage, the history of the network is partly accounted for by the biased percolation model.

The effect of the atomic back-flow, which contrasts the EM, is simulated by introducing a recovery process consisting in a stochastic healing of the broken resistors.[28,49,50] Therefore, the transformation $r_{OP} \rightarrow r_{reg,n}$ is allowed with probability

$$W_{R,n} = \exp[-E_R/k_B T_n], \tag{7}$$

where E_R is a recovery activation energy. Furthermore, the variation of the line composition due to alloying effects is described by allowing the stochastic transitions:[28] $r_{reg,n} \rightarrow r_{imp}$ and $r_{imp} \rightarrow r_{reg,n}$, occurring with probabilities $W_{RI,n} = \exp[-E_{RI}/k_B T_n]$ and $W_{IR,n} = \exp[-E_{IR}/k_B T_n]$, respectively, where E_{RI} and E_{IR} are two characteristic activation energies. By adopting this description of alloying effects, we are limiting ourself to consider the change in the elementary resistances due to a variation inside any grain or cluster of grains (single resistor) of the number of Cu atoms dispersed in the matrix or present in small $CuAl_2$ precipitate.[28]

The initial configuration of the RN can contain some initial concentrations of broken and impurity resistors, p_{ini} and p_{ini}^{imp}, respectively. Alternatively this initial configuration can be chosen as the perfect one: $p_{ini}=0$ and $p_{ini}^{imp}=0$. The network evolution is obtained by Monte Carlo simulations which are carried out according to the following iterative procedure.

(i) Starting from the initial network, we calculate $\{i_n\}$ and the network resistance R by solving Kirchhoff's loop equations. Moreover, we calculate $\{T_n\}$ by using Eq. (4).

(ii) OP and r_{imp} are generated with the corresponding probabilities W_{OP} and W_{RI} and the remaining r_{reg} are changed according to $\{T_n\}$. Then $\{i_n\}$ and $\{T_n\}$ are recalculated.

(iii) OP and r_{imp} are recovered with probabilities W_R and W_{IR}, respectively, and the resistances r_{reg} are changed again according to $\{T_n\}$.

(iv) $\{i_n\}$, $\{T_n\}$ and R are recalculated.

This procedure is iterated from (ii), thus the loop (ii)–(iv) corresponds to an iteration step, which is associated with a unit time step on an arbitrary time scale to be calibrated by comparison with experiments. Depending on the parameter values, which are related to the physical properties of the line and to the external conditions, the two following possibilities can be achieved during the iteration procedure: irreversible failure or steady-state evolution. In the first case, at least one percolating cluster of broken resistor (i.e., a cluster connecting the top and the bottom of the network) is formed and thus the resistance R diverges.[32] In the second case, the network resistance fluctuates around an average value $\langle R \rangle$ (saturation value).[49,50] The average over the statistical ensemble (different realizations of the failure of networks with the same parameters and in the same external conditions) of the values of the fraction of broken resistors corresponding to the appearance of at least one percolating cluster, is called the percolation threshold and it is denoted as p_c.[32]

To check the model we have considered EM tests performed with a standard median time to failure technique[1,2] on Al-0.5%Cu lines. The tests have been carried out at different currents and temperatures by adopting a 2-metal level configuration with tungsten vias[1,2] and by using a 20% relative resistance variation as the failure criterion. The lines used in the tests were 3000 μm long, 0.45 μm wide and 0.8 μm thick. The last thermal treatment undergone by these lines occurred during fabrication and it consisted of a high temperature annealing followed by a rapid cooling. This treatment left a nonequilibrium concentration of Cu dissolved into the Al matrix. Therefore, in the early stage of the EM test, the heating associated with the stress conditions gives rise to a formation of $CuAl_2$ precipitates. The low resistivity of these clusters and, mainly, the reduction of the internal disorder, i.e. the reduction of the number of scattering centers of Cu in the solid solution, cause an initial decrease of the line resistance.[11] Here, we consider the data obtained at $T=492$ K, shown in Ref. 28, and the data obtained at $T=467$ K, reported in the following section. In both cases the stress current density was $j=3$ MA/cm^2. The resistance of the lines at the reference temperature $T_{ref}=273$ K was $R_{ref}^{line}=269\ \Omega$ (averaged over a family of 40 samples), while the TCR was 3.6×10^{-3} K^{-1}.

The values of the parameters used in the simulations have been chosen as follows. We have taken the values corresponding to the actual stress conditions and to the physical parameters of the metallic line whenever possible, i.e., whenever it was possible to make a direct correspondence with the model parameters and the line properties and when this choice was not too heavy computationally. The remaining parameters have been chosen to fit the experimental results and/or to reduce the computational effort. Concerning this point, we notice that the present approach allows for a direct simulation of lines with ratio L/W up to ≈ 150. To describe the resistance evolution of lines characterized by higher values of this ratio, as the lines tested in the experiments shown in the next section (where $L/W=6667$), we have adopted the following further approximation. The network is taken to represent the region of dominant void growth inside a longer line, i.e., the region responsible for the resistance variation of the line. We can take the length of this region given by L/F, where F is an integer number. Thus, in the initial conditions, $R_{0,line}=FR_0$. On the other hand according to the above assumption we have $\Delta R_{line}=\Delta R$. Therefore, the relative resistance variation of the whole line can be expressed as $\Delta R_{line}/R_{0,line}=(1/F)(\Delta R/R_0)$. We underline that this approximation is used only to check the model by a direct comparison of the measured resistance evolutions of long lines (Fig. 2, later) and the evolutions calculated by the present model (Fig. 3, later). All the other results concern short lines and do not make use of the above approximation.

Thus, except when differently specified, we have used the following values of the parameters: $N_W=12$, $N_L=400$, $F=1$, $T_0=492$ K, $I=JWt_h=10.8$ mA (which corresponds to the values of j, W and t_{th} used in the EM tests cited above), $\alpha=3.6\times10^{-3}$ K^{-1}, $T_{ref}=273$ K, $r_{ref}=0.048\ \Omega$, $r_{imp}=0.016\ \Omega$. For the long lines used in the EM tests, when $F=200$, this value of r_{ref} provides the correct value for R_{ref}^{line}, reported above. Moreover, we have taken $A=2.7\times10^8$ K/W. According to Eq. (5), this value of A provides an initial heating of the network of 8.3 K, comparable with that estimated in the

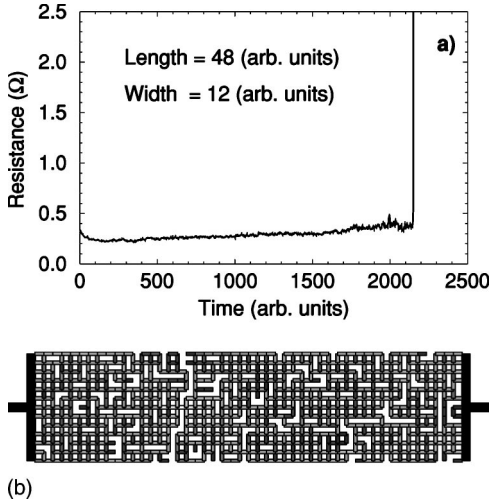

FIG. 1. (a) Typical resistance evolution of a 12×48 network. The values of all the other parameters are specified at the end of Sec. II. The stress conditions are $I=10.8$ mA and $T_0=492$ K. The resistance is expressed in Ohm and the time in arbitrary units corresponding to the number of iteration steps. (b) Damage pattern at the iteration step $t=2150$ of the evolution shown in (a). The different gray levels, from black to white, are associated with different T_n values, ranging from 492 to 700 K with a step of 10 K.

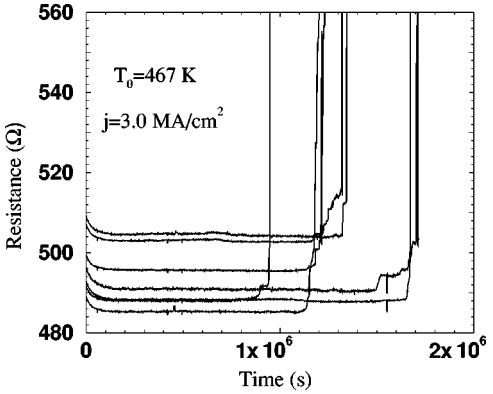

FIG. 2. Experimental resistance evolutions of seven Al-0.5%0.5Cu lines stressed at $T=467$ K by a current density $j=3$ MA/cm^2 (which corresponds to $I=10.8$ mA within the model). The resistance is expressed in Ohm and the time in seconds.

experiments of Ref. 28. The initial network configuration corresponds to $p_{ini}=0$ and $p_{ini}^{imp}=0$. Furthermore, we have taken $E_{OP}=0.41$ eV and $E_R=0.35$ eV as reasonable values for the activation energies E_{OP} and E_R. We notice that the value of E_{OP} controls the range of the time scale, nevertheless this range is in any case arbitrary within our model. Thus, the value of E_{OP} can be considered as a free parameter which can be chosen with the purpose of saving computational time. More crucial is the choice of E_R, whose value sets the importance of the recovery process,[49] i.e. the strength of the atomic back-flow due to the mechanical stress. Consequently with this choice of E_{OP} and E_R, the values of E_{RI} and E_{IR} have been taken sufficiently small to account for the separation of the temporal scales of the void formation and of the alloying processes, observed in the experiments. Here, we have taken $E_{RI}=0.22$ eV and $E_{IR}=0.17$ eV.

III. RESULTS

A. Resistance evolution

A typical resistance evolution and the corresponding damage pattern near the final failure are reported in Figs. 1(a) and 1(b), respectively. In this case $N_L=48$ while all other parameters take the values specified at the end of the previous section. In Fig. 1(a) we observe a resistance drop at the early stages of the evolution due to the generation of impurity resistors. This process $r_{reg,n}\rightarrow r_{imp}$ simulates the variation of composition of the line associated with the initial precipitation of part of the Cu dissolved in the Al matrix, as discussed in Sec. II. On the other hand, this process together with the antagonist one, $r_{imp}\rightarrow r_{reg,n}$, takes place on a time scale that is much shorter than that associated with the generation of broken resistors. Therefore, after a given amount of time (relaxation time of the alloying process), the concentration of the impurity resistors reaches its steady-state value[28] corresponding to the temperature $T_0+\Delta T$. On a longer time scale, the fraction of broken resistors increases and the network becomes more and more unstable. This implies an increase of both the resistance value and the resistance fluctuations, as shown in Fig. 1(a). Finally, at a given time (time to failure) the fraction of broken resistors reaches the percolation threshold and $R(t)$ diverges. Figure 1(b) reports the damage pattern just before the final failure. Precisely, this figure shows the temperature distribution inside the network: the broken resistors are the missing ones while the different gray levels, from black (cold) to white (hot), correspond to different T_n values ranging from the substrate temperature up to 700 K, with a temperature step of 10 K. The damage pattern mainly consists of a channel of broken resistors elongated in the direction perpendicular to the current flow, a characteristic feature of the biased percolation.[36,37] This simulated damage pattern reproduces well the experimental pattern observed by scanning electron or x-ray microscopy in metallic lines which are failed due to EM.[1,2,15,16]

Figure 2 shows the resistance evolutions of seven Al–0.5%Cu lines measured in the EM tests performed at $T=467$ K, as described in Sec. II. These lines were stressed by a current density $j=3$ MA/cm^2 which corresponds to $I=10.8$ mA. Figure 3 reports the resistance evolutions obtained by simulations. Here, different curves correspond to different realizations of failure. In this case, we have taken $N_W=12$, $N_L=400$, $F=200$, $T_0=467$ K, $r_{ref}=0.044\ \Omega$, $r_{imp}=0.006\ \Omega$, $p_{ini}=(2.5\pm0.2)\times10^{-2}$ (the broken resistors in the initial network configuration are supposed uniformly distributed), while the remaining parameters have the same values specified at the end of Sec. II. The time scale in Fig. 3 has been calibrated according to the following procedure. The statistical sample tested in the experiments was composed by thirteen lines and the resulting median time to failure, t_{50}, was: $t_{50,exp}\approx1.3\times10^6$ s. A sample of thirteen simulated failure realizations was considered and the corresponding $t_{50,sim}$ was calculated in units of iteration steps. From these two values, we obtained the value $\Delta t=185$ s for the time interval

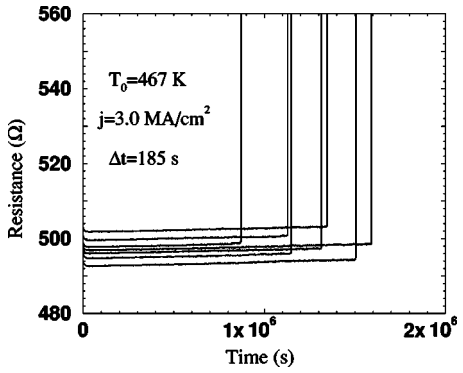

FIG. 3. Calculated resistance evolutions of the Al-0.5%Cu lines in Fig. 2. The simulations have been performed by taking $T_0=467$ K and $I=10.8$ mA. The value of the remaining parameters are specified in the text. The resistance is expressed in Ohm and the time in seconds by using the value $\Delta t=185$ s for the time interval associated with each iterative step (see the text).

to be associated with each iterative step. The comparison between Figs. 2 and 3 shows that the calculated evolution of the resistance well reproduces the main features of the observed evolution. We note that a small discrepancy between measured and simulated evolutions appears just before the failure, where the abrupt increase of the resistance shown by the simulated curves contrasts with a pre-failure increase of the resistance generally present in the experimental ones. This discrepancy is partly due to the factor $1/F$ relating the relative resistance variation of the network with that of the metallic line. In fact, the simulated evolutions obtained for short lines, see Fig. 1(a), when the full metallic line can be directly simulated and the approximation adopted for long lines can be avoided (i.e., $F=1$), also display a pre-failure region.

The agreement is further confirmed by the comparison between the distributions of the measured and calculated TTFs reported in Fig. 4. This figure shows on a lognormal plot[51] the cumulative distribution function (CDF) of the failure probability as a function of the times to failure obtained from the EM tests (full circles) and simulations (open circles) considered above. The agreement between experiments and simulations is excellent and the shape factor of the two distributions is $s=0.16$ in both cases. Thus, the direct comparison of the results of the model and of the EM tests, shown in Figs. 2–4, validate the present computational approach for the study of EM failures.

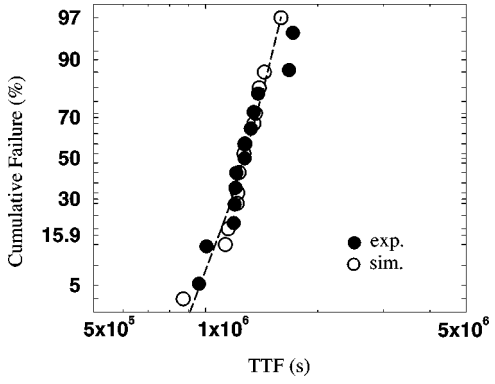

FIG. 4. Lognormal plot of the cumulative distribution function of the failure probability (expressed in percentages) as a function of the time to failure: (full circles) TTFs experimentally measured and (open circles) calculated by the model. The data correspond to the same statistical samples considered in Figs. 2 and 3, respectively. The stress conditions are $T_0=467$ K and $I=10.8$ mA. The dashed line fits the CDFs with a lognormal distribution.

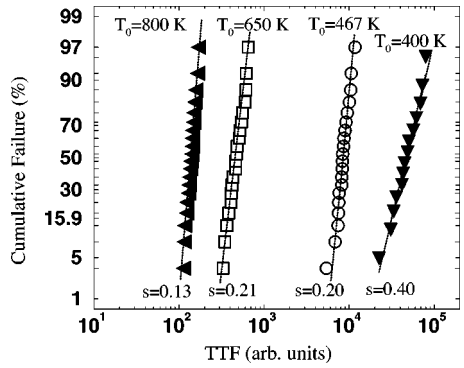

FIG. 5. Lognormal plot of the cumulative distribution functions of the failure probability (expressed in percentage) as a function of the time to failure. The different functions are calculated at different substrate temperatures: $T_0=800$ K (triangles left), $T_0=650$ K (open squares), $T_0=467$ K (open circles), $T_0=400$ K (triangles down). The stress current is $I=10.8$ mA. The solid lines fit the CDFs with lognormal distributions.

As anticipated in Sec. I, two central problems encountered in the study of EM phenomenon concern the role played by the stress conditions and the line geometry on the damage process.[1,2,27] Therefore, with the purpose of further checking the predictivity of the model and of extracting new information from it, we have calculated the effect on TTFs of temperature, stress current, length and width of the lines. To contain the computational effort and to avoid the approximation used for long lines, the study has been limited to short or moderately short lines. Thus, in the following we will discuss the results of simulations carried out by taking $F=1$, by varying T_0, I, N_L, N_W, while keeping all the remaining parameters to the values specified at the end of Sec. II.

B. Stress conditions: Temperature and current effect

We start by considering the effect of temperature on the times to failure of 20 networks of sizes 12×400 stressed by a current of $I=10.8$ mA. Accordingly, we analyze the dependence on temperature of t_{50} and s, the two parameters which determine a lognormal distribution. We consider fourteen values of T_0 ranging from 400 K to 800 K, a considerably wider range with respect to standard accelerated tests.[1,2] Figure 5 shows the cumulative distribution functions of the failure probability calculated for $T_0=800$ K (triangles left), $T_0=650$ K (open squares), $T_0=467$ K (open circles) and $T_0=400$ K (triangles down), while the solid lines fit the CDFs with lognormal distributions. These four T_0 values are selected as representative for the behavior of s. Indeed, we have found that s is nearly independent of temperature in a wide range of intermediate temperature values, while it in-

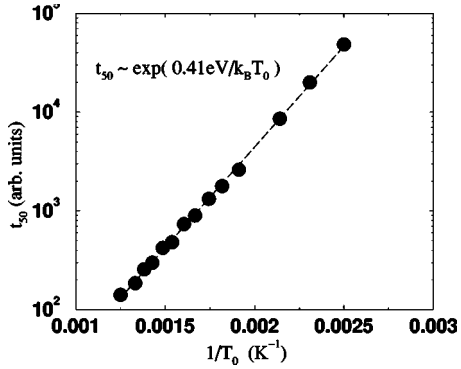

FIG. 6. Median time to failure, t_{50}, as a function of the inverse substrate temperature. The median times to failure are expressed in arbitrary units and the temperature in K. The stress current is $I=10.8$ mA. The dashed line is the fit with the exponential function $Z\exp[4700/T_0]$.

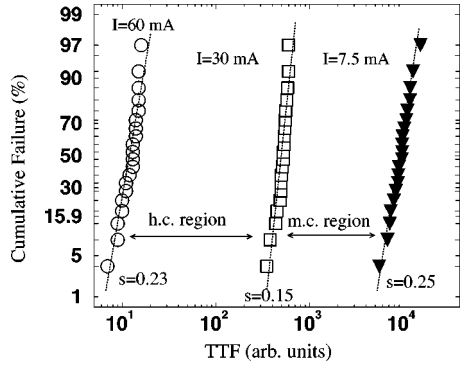

FIG. 7. Lognormal plot of the cumulative distribution functions of the failure probability (expressed in percentage) as a function of the time to failure. The different functions are calculated at different stress currents: $I=7.5$ mA (triangles down), $I=30.0$ mA (open squares), $I=60.0$ mA (open circles). The substrate temperature is $T_0=492$ K. The solid lines fit the CDFs with lognormal distributions.

creases significantly at low temperatures and decreases at the highest temperatures considered here. The broadening of the distribution at low temperatures and its narrowing at high temperatures witness the different importance of the network microgeometry in the two extreme stress conditions of 400 and 800 K, respectively. Indeed, the network microgeometry, resulting from the stochasticity of the defectiveness, give rise to a kind of network individuality. At very high stress, the differences in the network microgeometry loose their importance. The contrary occurs at low stress, where this diversity becomes of importance in determining the actual TTF. We underline that the broadening of the TTF distribution at low temperatures has important implications in the interpretation and use of the results of accelerated EM tests. In fact, when evaluating the reliability of a family of lines under standard operating conditions (usually close to room temperature and relatively low current density), it is crucial to estimate not only t_{50} but also the minimum time to failure.[7,8] The determination of these two quantities is usually obtained from accelerated tests performed at high temperatures on a statistically significant, but in any case small, sample of the entire family. Then, the estimate of the minimum time to failure of the family is obtained by an extrapolation of the CDF in the region of low failure probability.[7,8] Such an estimate is very sensitive to a possible broadening of the TTF's distribution at the operation temperature. For this reason it is crucial to estimate and to take into account the dependence of s on temperature. We remark that the increase of s at low temperatures is a source of the following apparent paradox:[8] the minimum time to failure at low temperatures can be shorter than the minimum time to failure at high temperatures. We will face a similar paradox by discussing the dependence of s on the current.[8] Solutions to this apparent paradox has been proposed in the literature,[8,14] based on the necessity of testing large samples and on the introduction of a three parameters lognormal distribution, where the third parameter is a characteristic incubation time.[8]

The analysis of the temperature dependence of the TTFs is completed by Fig. 6 which displays on a linear-log scale the calculated values of t_{50} as a function of the inverse of the substrate temperature. Here, the dashed line is the best fit obtained with the function $Z\exp[E/k_B T_0]$, where Z is a fitting amplitude. Thus, the calculated values of t_{50} perfectly follow, within the numerical uncertainty, the Black's law[1,2,26] discussed in Sec. I. The value of E extracted from the fit is $E=0.41$ eV; thus $E=E_{OP}$, and we can identify the activation energy of the resistor breaking process with the EM activation energy.

To investigate the effect of current on the failure process, we have calculated the TTFs of 12×400 networks stressed at $T_0=492$ K by different (thirteen) current values in the range 5.0–60 mA. For each current value s and t_{50} have been determined by considering twenty realizations of failure. Figure 7 shows the CDFs of the failure probability versus failure time, calculated for $I=7.5$ mA (triangles down), $I=30$ mA (open squares), $I=60$ mA (open circles). The solid lines fit the CDFs with lognormal distribution. We have found that the shape factor of the distribution exhibits a minimum at intermediate values of I. Thus, we can identify two regions of current values: a moderate current (m.c.) region, where s decreases at increasing current, and a high current (h.c.) region, where s increases at increasing current. Such a broadening of the TTF's distribution at low currents has been actually observed in several EM tests.[7,8] Its implications concerning the evaluation of the reliability of metallic lines are similar to those previously mentioned in connection with the effect of temperature. A detailed discussion of these problems can be found in Ref. 8. Here, we underline that the non-monotonic behavior of s versus current contrasts the general monotonic behavior found versus temperature. This non-monotonic behavior of s can be understood by considering also the dependence of t_{50} on the current that is reported in Fig. 8. More precisely, we show in the inset of this figure a log-log plot of the calculated values of t_{50} versus I. We can see that t_{50} exhibits two power-law regions. A first one is in the moderate current region and is characterized by a current exponent $n=2.1$, in good agreement with Black's law.[17,26] A second power-law with a higher exponent, $n=5.7$, is found in the high current region. We notice that similar behaviors at high current densities have actually been

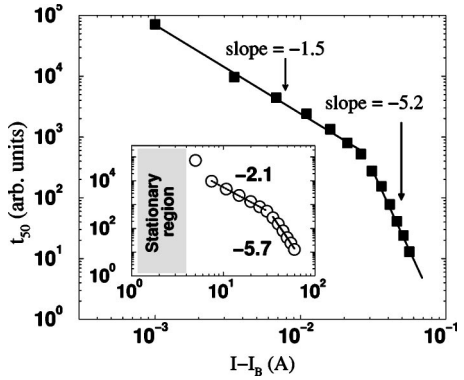

FIG. 8. Log-log plot of t_{50} versus $I-I_B$, where I_B is the breakdown current defined in the text. The two lines of slope −1.5 and −5.2 represent the fits with a power-law in the moderate current and in the high current regions, respectively. The inset shows the log-log plot of t_{50} versus I. In both the main figure and the inset, the median times to failure are expressed in arbitrary units and the current in mA. The gray region in the inset corresponds to the stationary region attainable for currents lower than the I_B value.

observed in EM measurements and are frequently reported in the literature.[1–3] Furthermore, the same inset of Fig. 8 shows that t_{50} drastically increases at the lowest currents. Here, for $I=4.0$ mA the networks are found to remain stable over more than 5×10^5 iterations. This strong increase of t_{50} is associated with the existence of a threshold current, I_B, below which a steady state condition is achieved, manifesting itself in a saturation of the network resistance. Accordingly, for $I<I_B$ the electrical breakdown no longer occurs. For this reason, in Fig. 8 the region corresponding to $I<I_B$ is evidenced in gray. Previous investigations of the general properties of the model, reported in Refs. 49, have shown the existence of this threshold. Some of the properties of the steady state of the network will be discussed later in connection with the results concerning resistance noise and we refer the reader to Refs. 49 for a deeper analysis of these properties. We emphasize that this sharp increase of t_{50} at low currents has also been observed in EM tests.[2,7] Therefore, the dependence of t_{50} on the current obtained by simulations agrees with the behavior measured over the full range of current values. To complete the analysis, Fig. 8 reports in a log-log plot the median time to failure versus the difference $I-I_B$ (full squares). By taking for I_B the value given above, $I_B=40$ mA, we have found that t_{50} scales as

$$t_{50}\sim(I-I_B)^{-n_g}. \tag{8}$$

This expression, first proposed by Filippi *et al.*,[7] can be considered as a generalization of Black's law and n_g can be called as generalized current exponent, to distinguish it from the current exponent n of the conventional Black's law, Eq. (1). Figure 8 displays two current regions, each characterized by a given value of n_g. These two regions correspond to the different current dependence of the distribution shape factor, reported in Fig. 7. The common behavior of t_{50} and s with current originates from the change with the bias of both the damage pattern and the magnitude of Joule heating and can be understood as follows.

First, let us consider a simpler system: a network in which two stochastic processes of resistor breaking and recovery occur with uniform probabilities: $W_{D0}=\exp[-E_{OP}/k_BT_0]$ and $W_{R0}=\exp[-E_R/k_BT_0]$. A similar network, subjected to random percolation[32,52] describes well the instability of very thin metallic films due to agglomeration phenomena.[53] The stability of this network has been studied in Ref. 52 where the failure condition and the expression for the average time to failure[54] (ATTF) have been derived in the limit of networks of infinite size. Here, to point out the dependence of the percolation threshold on the system size, it is convenient to write the failure condition in the following form:

$$W_{D0}>\frac{p_c}{(1-p_c)}\frac{W_{R0}}{(1-W_{R0})}; \tag{9}$$

similarly, the average time to failure can be written as

$$\mathrm{ATTF}=\frac{\ln(1-q)}{\ln[(1-W_{D0})(1-W_{R0})]}, \tag{10}$$

with

$$q\equiv p_c\left[1+\frac{W_{R0}}{W_{D0}(1-W_{R0})}\right], \tag{11}$$

where $q<1$ for failing networks, according to Eq. (9). For this simple system it is quite easy to determine the role of the size and of the geometry of the network on the value of the percolation threshold. In fact, an ideally infinite network ($N_L\to\infty$ and $N_W\to\infty$), with percolation threshold $p_{c,\infty}$, would have a zero probability of breaking for a fraction of defects $p<p_{c,\infty}$ and a breaking probability equal to 1 for $p>p_{c,\infty}$.[32] However, for networks of finite size there is a nonvanishing probability of formation of the percolating cluster of defects (thus, of breaking) also when the defect fraction is $p<p_{c,\infty}$ and, for contrast, a probability less than 1 for $p>p_{c,\infty}$.[32] For this reason, when networks of finite size are considered, p_c is defined as the average over the statistical ensemble of the minimum values of p corresponding to the formation of at least one percolating cluster,[32] as anticipated in Sec. II. In the case of $N\times N$ networks with N finite, it has been found[32] that $(p_c-p_{c,\infty})=cN^{-1/\nu}$, where ν is the correlation length exponent (with universal value $\nu=4/3$ in two-dimensions), while the proportionality constant, c, depends on the lattice structure. In particular, for networks with a square-lattice structure, it has been found[55] that $c\approx0$ and thus $p_c\approx p_{c,\infty}=0.5$, independently of N. In the case of rectangular $N_W\times N_L$ networks with a square-lattice structure, we have found that for a fixed value of N_W, p_c decreases with N_L, by reaching its minimum value, $p_{W,\infty}$, when $N_L\to\infty$. More precisely, $(p_c-p_{W,\infty})\sim N_L^{-1/2\nu}$, where $p_{W,\infty}$ decreases with N_W. The reduction of p_c when increasing the length, by keeping constant the width of the network, can be explained as a consequence of the existence of a higher number of possible paths of defects connecting the top and the bottom of such a network compared to a square network with the same width. These feature is associated with the greatest instability of networks with this geometry.

We note that Eqs. (9)–(11) and the subsequent discussion apply to the case of random percolation, therefore the aver-

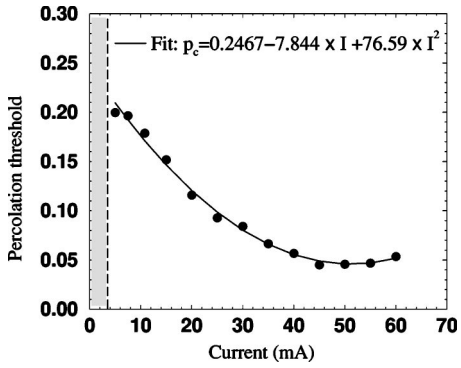

FIG. 9. Percolation threshold for broken resistors, p_c, versus current (this last is expressed in mA). The curve is a quadratic fit (see the text). The gray region evidences the stationary region.

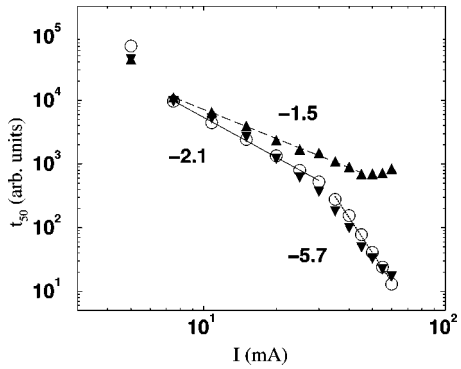

FIG. 10. Log-log plot of t_{50} versus I. The median times to failure are expressed in arbitrary units and the current in mA. The open circles (from MC simulations) represent the same data reported in the inset of Fig. 8. The up-triangles are obtained by Eq. (10) but taking into account the dependence $p_c(I)$ shown in Fig. 9. The down-triangles are obtained with the same procedure but replacing the probabilities W_{D0} and W_{R0} with $\langle W_{OP}\rangle$ and $\langle W_R\rangle$. The solid, long-dashed and dotted curves represent the best-fit with a power-law with slopes −2.1, −1.5, −5.7, respectively.

age time to failure given by Eq. (10) is independent of the current. On the other hand, electromigration is a current driven phenomenon which, within our approach, is described by a biased percolation.[36,37] The effect of the biased percolation can be roughly decomposed in two components: (i) a correlated growth of the defect pattern, which exhibits an increasing degree of filamentation at increasing currents; (ii) an average heating of the network due to the Joule effect.

The filamentation driven by the external current implies a bias dependent percolation threshold $p_c(I)$, as shown in Fig. 9. In this figure the full circles represent the values of the percolation threshold calculated by averaging the fraction of defects which corresponds to the failure of 20 networks of sizes 12×400 subjected to external currents $I>I_B$. The gray region in Fig. 9 corresponds to values $I<I_B$ (stationary region), while the solid curve is the best-fit with a quadratic expression. We notice that for low currents the defect pattern is found to exhibit a relatively week degree of filamentation and the value of $p_c=0.21$ is not very far from the random percolation threshold (which, for these values of N_W and N_L, is $p_c=0.37$). Then, for currents up to $I\approx 40$ mA the filamentantion achieves its maximum level and consequently p_c its minimum value. At further increasing I values, the onset of a multi-filamentation pattern is observed[56] with the simultaneous growth of several filaments of defects (voids) elongated perpendicular to the direction of the current flow.[56] This effect manifests itself in a smooth increase of the percolation threshold at the highest currents, as shown in Fig. 9.

By introducing the above dependence of p_c on I in Eqs. (10) and (11) we obtain the average time to failure versus current shown in Fig. 10 (up-triangles). For the sake of comparison, we also show in this figure (open circles) the values of t_{50} obtained by MC simulations and already reported in the inset of Fig. 8. We can see that at low currents the ATTFs obtained from Eq. (10) by accounting for the bias driven filamentation, tend to merge with the MC results. Then, in the moderate current region the ATTF exhibits a power-law behavior, with a current exponent $n=1.5$ (the dashed curve in Fig. 10 is the best-fit with such a power-law). Finally, for currents $I\approx 40$ mA the ATTF nearly saturates. The discrepancy at intermediate and high currents between the two sets of data [ATTFs from Eq. (10) and MC simulations] can be explained in terms of Joule heating effects. These effects can be included in Eq. (10), in the spirit of a mean field theory, by replacing in the random percolation expressions of the breaking and recovery probabilities, the temperature T_0 with an average temperature $\langle T\rangle = T_0+\Delta T$, where ΔT is given by Eq. (5). By introducing into Eq. (10) these new average probabilities $\langle W_{OP}\rangle$ and $\langle W_R\rangle$ and by simultaneously accounting for the dependence $p_c(I)$, we obtain the average time to failure reported as down-triangles in Fig. 10. Thus, the up-triangles in this figure correspond to a value of the structure thermal resistance $\theta=0$ and the down triangles to $\theta\neq 0$. The excellent agreement found between MC results and those obtained through Eq. (10) supports the interpretation suggested here. Thus, the generalization of Eq. (10) to the case of biased percolation, made by accounting for both Joule heating effects and for the dependence of the percolation threshold on the bias, is able to describe quite well both the results of the MC simulations and the behavior observed in many EM experiments.[1–3,7]

The results reported in Fig. 10 shed new light on the role played by Joule heating effects in determining the value of the current exponent in Black's law. Indeed, though many accelerated EM tests[1–3] provide a value of $n=2$, other values of n have been frequently measured.[1–3,23] Values of n greater than 2 have been usually attributed to Joule heating.[1–3,23] In this respect, Fig. 10 points out quite well the importance of this effect in the high current region, thus confirming the interpretation made in the literature. However, Fig. 10 shows that Joule heating can affect the value of n also in the moderate current region. In this region values $1<n<2$ have been reported by different authors.[1,2,23] Many EM models have been proposed to explain the value of the current exponent.[1,2,17,23] These models fall into two main categories: "void growth" and "nucleation" models.[23] In the void growth models, the failure is taken to occur after a void grows up to a critical size. It is generally accepted that this category of models provides a value $n=1$.[23] In nucleation models, the failure arises from the buildup of a critical vacancy concen-

tration. It is generally believed that this second category of models provides a value $n=2$.[17] Recently, Tammaro and Setlik[23] have proved that even when nucleation is the limiting process it can be $1<n<2$. Our results confirm this conclusion. As a matter of fact, the present model, which relates the failure to the achievement of a percolation threshold for the defect fraction, belongs to the second category of models. In fact, as shown by Fig. 10, metallic lines with different structure thermal resistance θ, thus exploiting different sensitivity to Joule heating effects, can exhibit different current exponent values, even in the moderate current region. Concerning this point, we underline the fact that a power-law behavior of the ATTF versus current is predicted by the model merely as a consequence of the filamentation of the damage pattern, even neglecting the effect of the average heating of the metallic line. Moreover, the dependence of n on the length of the lines, reported in EM tests,[3] can be explained in terms of dependence of both, heating effects and p_c, on the length of the system. Finally, from Fig. 10 we can see that Joule heating is also responsible for the shift towards lower current values of the crossover between the high-current and the moderate-current regions (in this case from 40 mA to 30 mA). On the basis of the above considerations we can now understand the dependence with current of the shape factor of the TTFs distribution shown in Fig. 7. At relatively low currents, just above the I_B threshold, the degree of filamentation of the defect pattern is weak and there is a wide spread in the network microgeometries and thus in the TTFs. Then, at increasing currents, the degree of filamentation increases and the effect of the different network microgeometries is reduced together with the spread in the TTFs. Finally, in the highest current region, because of strong Joule heating, multi-filamentation occurs.[56] This implies a high degree of stochasticity and in turn a high variability of microgeometries together with an increase of the TTFs spreading.

C. Geometrical effects

In this section we investigate the effect of the length and width of the network on the failure process. First, we have analyzed the dependence of t_{50} on the length N_L of the network. Figure 11 displays the simulated median time to failure as a function of N_L. The data indicated by full circles are obtained by taking $N_W=12$ and $I=10.8$ mA, while the data reported as open squares and shown in the inset of Fig. 11 correspond to $N_W=36$ and $I=32.4$ mA. Thus, in both cases the current density (measured in current units)[57] is $j=I/N_W=0.9$ mA. We have found that t_{50} sharply increases by decreasing N_L and it diverges for network lengths below a certain value, N_{L_c}. This length can be considered as a critical length of the network and it is dependent on the network width, as shown in Fig. 11. Furthermore, for sufficiently long networks, t_{50} nearly saturates to a value independent of the length and increasing when increasing the width. In the following, this asymptotic value of the median time to failure in the limit of infinitely long lines will be denoted as t_{inf}. The behavior of t_{50} shown in Fig. 11 is in qualitative good agreement with the behavior observed in the EM experiments.[2]

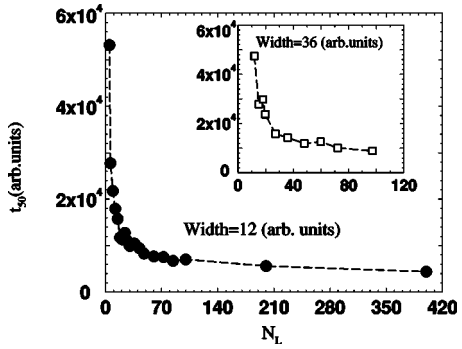

FIG. 11. Median time to failure, t_{50}, as a function of the network length N_L for $N_W=12$ and $N_W=36$ (inset). The median time to failures are expressed in arbitrary units. The dashed lines are a guide to the eyes.

To determine more precisely the dependence of the median time to failure on the geometrical parameters, we have analyzed the simulated values of t_{50} as a function of the difference $(N_L-N_{L_c})$. Figure 12 reports the log-log plot of the difference $t_{50}-t_{inf}$ as a function of the difference $(N_L-N_{L_c})$. Here, together with the data already shown in Fig. 11 we have also reported the data for $N_W=48$ and $I=43.2$ mA (open circles). In this way, all the data in Fig. 12 correspond to the same value of j. We have found the following values of critical length: $L_c=2.5$, 7.5, 10.0, for $N_W=12$, 36, 48, respectively. Therefore, in all the cases it is $(N_{L_c}/N_W)=0.21\pm0.01$. The values of t_{inf} range between $2\times10^3-3\times10^3$. Figure 12 shows that the difference $t_{50}-t_{inf}$ follows a power-law as a function of the difference $(N_L-N_{L_c})$; indeed, the solid, dashed and long dashed curves in this figure fit the data with a power-law with exponent $-\lambda$, where $\lambda=0.62\pm0.02$. In particular, as shown in the inset of Fig. 12, we have found that the three sets of data collapse onto the same curve once the difference $t_{50}-t_{inf}$ is considered as a function of the normal-

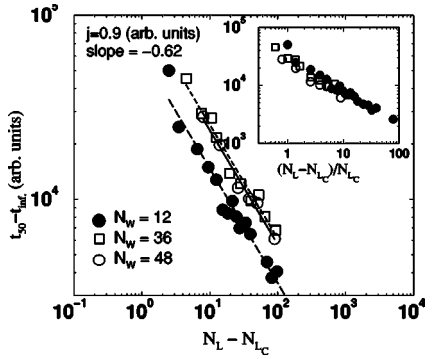

FIG. 12. A log-log plot of the difference $t_{50}-t_{inf}$ versus the difference $(N_L-N_{L_c})$, where t_{inf} is the median time to failure in the limit of infinitely long lines and N_{L_c} is the critical length. Both quantities are expressed in arbitrary units. The full circles are obtained by taking $N_W=12$, $I=10.8$ mA. In this case is $N_{L_c}=2.5$. The open squares correspond to $N_W=36$, $I=32.4$ mA and $N_{L_c}=7.5$ while the open circles to $N_W=48$, $I=43.2$ mA and $N_{L_c}=10.0$. The solid, dashed and long dashed curves fit the data with a power-law of exponent -0.62 ± 0.02. In the inset the same data of $t_{50}-t_{inf}$ are reported as a function of $(N_L-N_{L_c})/N_{L_c}$.

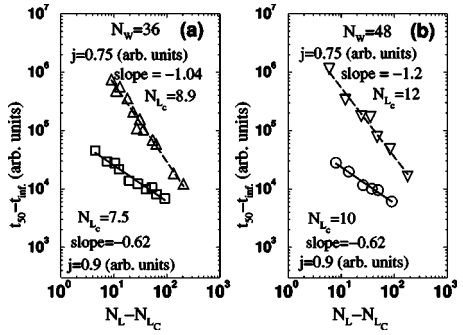

FIG. 13. (a) A log-log plot of the difference $t_{50}-t_{inf}$ versus the difference $(N_L-N_{L_c})$, where t_{inf} is the median time to failure in the limit of infinitely long lines and N_{L_c} is the critical length. Both quantities are expressed in arbitrary units. The network width is $N_W=36$. The open squares are obtained by taking $I=32.4$ mA, in this case $N_{L_c}=7.5$. The up-triangles correspond to $I=27.0$ mA and $N_{L_c}=8.9$. (b) $N_W=48$; open circles: $I=43.2$ mA and $N_{L_c}=10.0$; down-triangles: $I=36.0$ mA and $N_{L_c}=12.0$.

ized quantity $(N_L-N_{L_c})/N_{L_c}$. Thus, the difference $t_{50}-t_{inf}$ scales with the ratio $(N_L-N_{L_c})/N_{L_c}$:

$$t_{50}-t_{inf}\sim\left[\frac{N_L-N_{L_c}}{N_{L_c}}\right]^{-\lambda}\sim\left[\frac{N_L}{N_{L_c}}-1\right]^{-\lambda}. \qquad (12)$$

With the aim of identifying the physical parameters determining the value of λ, we have investigated the dependence of t_{50} on the length of the networks when these are stressed by different current densities. The results of simulations are reported in Figs. 13(a) and 13(b). Figure 13(a) displays the difference $t_{50}-t_{inf}$ versus $(N_L-N_{L_c})$ for $N_W=36$ and $j=0.9$ mA (open squares) and $j=0.75$ mA (up-triangles). The first set of data is the same of Fig. 12 (thus $N_{L_{c1}}=7.5$), while for the second set it is $N_{L_{c2}}=8.9$ and therefore $N_{L_c}/N_W=0.25$. First we note that it is

$$(jN_{L_c})_1\approx(jN_{L_c})_2, \qquad (13)$$

in agreement with Blech's law[1,2,27] (in this case we have obtained for the threshold product a value 6.8 mA). Second, we have found that the value of λ is different for the two sets of data. Precisely, for the data obtained by taking $j=0.75$ mA it is $\lambda=1.04\pm0.03$.

Figure 13(b) displays the difference $t_{50}-t_{inf}$ versus $(N_L-N_{L_c})$ for $N'_W=48$. The current densities $j=0.9$ mA (open circles) and $j=0.75$ mA (down-triangles) are the same of those in Fig. 13(a), while the values of the critical lengths are, respectively, $N'_{L_{c3}}=10.0$ and $N'_{L_{c4}}=12.0$. The value of the exponent found for $j=0.75$ mA is now $\lambda=1.20\pm0.04$. This result suggests a dependence of the exponent λ not only on j. We note that also for this set of data Blech's condition, Eq. (13), is satisfied with $(jN_L)'_c=9.0$ mA. Thus, by considering the threshold product as a function of the different parameters, $(jN_L)_c=F(r_0,N_W,E_R,T_0,\ldots)$, F is found to be an increasing function of N_W.

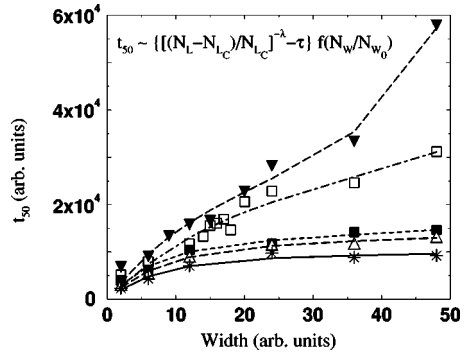

FIG. 14. A plot of t_{50} as a function of network width N_W. The different sets of data correspond to networks of different length: $N_L=15$ (down-triangles), $N_L=18$ (open squares), $N_L=36$ (full squares), $N_L=48$ (up-triangles), $N_L=100$ (stars). The curves fit the corresponding data with the expression specified in the text.

According to the model proposed by Blech,[27] the threshold product is determined by the ratio $(\Omega_a\Delta\sigma)/(\rho Z^*e)$ [Eq. (2) in Sec. I]. The quantity (ρZ^*e) is related to the intrinsic properties of the material and, within our model, can be associated with the parameter r_0, defined in Sec. II. On the other hand, the product $(\Omega_a\Delta\sigma)$, being a function of the geometry of the line, of the properties of the electrical contacts, of the presence of passivation layers and of the temperature,[1,2,9,27] within our model is controlled by the geometry of the network, by the efficiency of the recovery process (i.e., the energy E_R) and by the temperature T_0. In particular, according to Eq. (2), the value of the threshold product $(jL)_c$ is an increasing function of $\Delta\sigma$ which is the maximum value of the mechanical stress difference between the line terminals that the line can bear.[1,2,27] On the other hand, the value of this maximum stress difference increases with the line width. Therefore, the dependence of the threshold product on the width predicted by our model is in qualitative agreement with the behavior described by Eq. (2). In any case, further studies are necessary to determine the dependence of t_{inf}, λ and of the threshold product on r_0, N_W, E_R, T_0, and the other parameters of the model.

Below we analyze in more detail the dependence of the simulated median time to failure on the width of the network. To this purpose Fig. 14 reports t_{50} versus N_W for networks of different lengths, stressed by a current density $j=0.9$ mA. Going from the top to the bottom of the figure the different sets of data correspond to $N_L=15$, 18, 36, 48, 100, respectively. The different curves in Fig. 14 fit the corresponding data with the expression

$$t_{50}=K\left[\left(\frac{N_L-N_{L_c}}{N_{L_c}}\right)^{-\lambda}-\tau\right]F(N_W/N_{W0}), \qquad (14)$$

where $F(x)\equiv(1-e^{-x})$, $\lambda=0.62$, $N_{L_c}=0.21N_W$, $W_0=7-12$, τ is a constant related to the value of t_{inf}, and K is a fitting constant. As a general trend, t_{50} increases systematically at increasing the width of the network. However, in the case of long lines the dependence of t_{50} on the width shows a saturation at the largest width. By contrast, in the case of short lines this saturation disappears and t_{50} exhibits a final sharp

increase with the width and a tendency to diverge when approaching the Blech condition. This behavior of t_{50} is in overall agreement with the results of EM tests performed on lines larger than about 2 μm.[1,2] On the other hand, it has been found that narrow lines, with width smaller than 2 μm, exhibit a sharp lengthening of the median time to failure.[1–4] This phenomenon occurs because for such narrow lines (known as bamboo structures) the grain size becomes comparable with the line width.[1,2] As a consequence, the lack in these lines of grain boundaries along the direction of current implies that EM can only occur within the bulk of the grains or along interfaces. These processes usually require an activation energy significantly higher than that associated with EM along grain boundaries.[1,2] Therefore, bamboo structures exhibit median time to failure longer than that displayed by other kinds of lines.[1–4] Figure 14 shows that our model, in the present formulation, is unable to describe the lengthening of t_{50} for very narrow lines. This is not surprising considering the fact that here we have taken a single value for the activation energy of the breaking process, E_{OP}, that is a value common to all the resistors in the network. A further implementation of the model which introduces two different activation energies for the breaking of bulk resistors and surface resistors, $E_{OP,B}$ and $E_{OP,S}$ respectively, with $E_{OP,B} > E_{OP,S}$, would account also for this lengthening of t_{50} for narrow lines typical of bamboo structures.

D. Saturation and resistance fluctuations

In this section we consider the situation occurring at low current densities or for short line lengths, when the product of the current density and of the line length is lower than the threshold value. In this case electromigration stops and the resistance of the line achieves a steady state value (saturation value) dependent on the external conditions and on the properties of the line.[27,9] The steady state is characterized by fluctuations of the resistance around the average value $\langle R \rangle$ (this value is calculated by averaging over all the steady state values of the resistance, i.e., the values taken after the transient time associated with the termination of the EM process).[49] The study of resistance saturation effects and of their dependence on the stress current, temperature, geometry and other properties of the metallic line, can provide an important tool to investigate EM phenomena,[9] alternative to the study of the median time to failure. Actually, studies of EM based on saturation effects exhibit the advantage to be nondestructive and, in particular, they reveal their effectiveness in the analysis of short lines.[9] Furthermore, from a fundamental point of view, they provide the possibility to investigate fluctuation phenomena under far from equilibrium conditions.

Below we consider the steady state of networks biased by currents below the electrical breakdown threshold $I \leqslant I_B$. Figure 15 shows the resistance evolution of a 12×400 network with the same parameters considered in Sec. III B. More precisely, we report the difference $R(t) - R_0$ versus time for a network stressed at $T_0 = 492$ K by the current $I = 4.0$ mA which corresponds to the threshold for electrical failure. Saturation to $\langle R \rangle$ and large resistance fluctuations are well

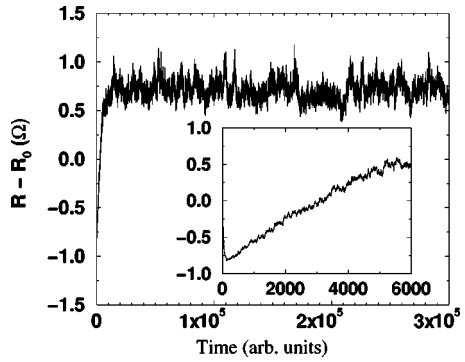

FIG. 15. $R(t) - R_0$ versus time for a network 12×400 stressed at $T_0 = 300$ K by a current $I = I_B = 4$ mA. Here R_0 is the perfect network resistance. The inset shows on an enlarged time scale the evolution of the resistance in the initial stage.

evident in Fig. 15 for this current value. The inset in this figure reports on an enlarged time scale the initial transient values of $R - R_0$, evidencing also the initial decrease of the resistance due to alloying effects, discussed in Sec. II. Details concerning the dependence of $\langle R \rangle$ on the value of the stress current, on the bias conditions (constant current or constant voltage) and on the TCR can be found in Refs. 49.

Here we discuss two important features of the resistance fluctuations occurring in a metallic line in a nonequilibrium steady state, stressed by a current near the EM threshold. First, we consider the non-Gaussianity property[58–60] of the distribution of $\delta R \equiv R - \langle R \rangle$. To this purpose, we have calculated the probability density function, Φ, of the distribution of δR for the steady state signal in Fig. 15. Figure 16 reports the product $\Phi\sigma$ as a function of $(\langle R \rangle - R)/\sigma$ in a lin-log plot, where σ is the root mean square deviation from the average resistance. For comparison, in the same figure we also report the Gaussian distribution (dashed curve), which in this normalized representation has zero mean and unit variance. This representation has been adopted because, by making the distribution independent of its first and second moments, it is particularly convenient for exploring the functional form of a distribution.[60] The results in Fig. 16 show a considerable non-Gaussianity of the distribution of δR, which is associated with the fact that the system is close to breakdown con-

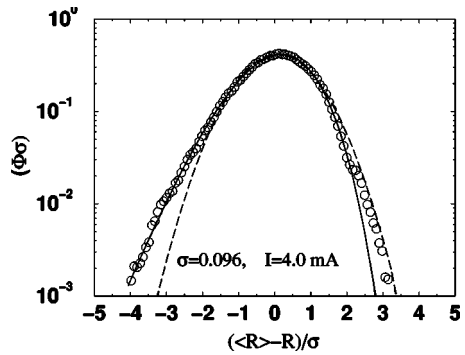

FIG. 16. Normalized probability density function, $F \equiv \Phi\sigma$, of the resistance fluctuations reported in Fig. 16. The solid curve fits the data with a generalized Gumbel distribution (see the text), while the dashed curve is the Gaussian distribution.

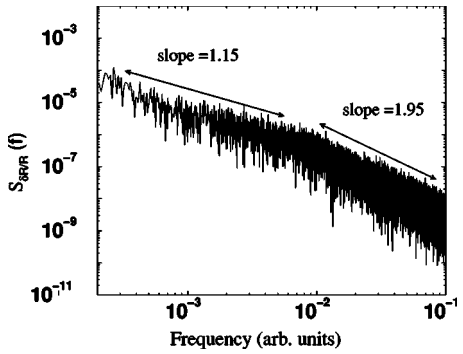

FIG. 17. The power spectral density of the resistance fluctuations in Fig. 16. The frequency and the spectral density are expressed in arbitrary units.

ditions. We have found that this non-Gaussianity is sufficiently well fitted by a generalized form[60] of the Gumbel distribution (solid curve), where this last is commonly used for the analysis of extreme events.[1] The role of the stress current and of the size of the system on the distribution of the resistance fluctuations has been studied in Refs. 61, where the conditions under which the distribution achieves the universal behavior described by the Bramwell, Holdsworth and Pinton distribution[60] have been identified.

As a second feature, we consider the power spectral density of resistance fluctuations. To this purpose, Fig. 17 displays the power spectrum associated with the steady state signal in Fig. 15. Both the frequency and the spectral density are expressed in arbitrary units. Two regions can be identified in the spectrum: a $1/f$ like branch at low frequencies and a Lorentzian cut-off at high frequencies. This feature is here interpreted as due to the presence of three relaxation mechanisms: (i) the slowest one related to the breaking and recovery of the regular resistors and describing the generation and recovery of microvoids; (ii) the fastest one associated with the transformation of regular resistors into impurity resistors (and *vice versa*) and describing alloying effects; (iii) an intermediate one corresponding to the generation and breaking of impurity resistors. Accordingly, the Lorentzian branch describes the evolution occurring on a fast scale when only the second transformation is present. On the slow scale, the other two transformations become of importance and thus all the relaxation mechanisms coexist. Therefore, a $1/f$-like spectrum appears in the low frequency region, in agreement with resistance noise measurements performed on Al–Cu alloys.[2,6,13] We notice that by taking different activation energies for bulk and surface resistors, as described at the end of Sec. III C, a further relaxation time would be added.

IV. CONCLUSIONS

We have applied the biased percolation model to the study of degradation and failure phenomena induced by EM in a metallic line. Our "coarse grain" approach focuses on the correlations established by the electronic current among the different elemental resistors of the network which mimic the structural components of the system (grains, clusters of grains, interfaces, etc. i.e., atomic transport channels). This approach provides a unified theoretical framework able to account successfully for many relevant features of the experiments, including the damage pattern, the resistance evolution, alloying effects and the statistical properties of TTFs. In particular, the model correctly predicts a lognormal distribution for TTFs, perfectly superimposing with the experimental one and it is able to estimate the dependence of the shape factor of the distribution on current and temperature. In what concerns the dependence of the median time to failure on the stress conditions, the model predictions agree with the experiments over the full range of current and temperature values considered. Simulations performed on rectangular networks of different length and width have allowed us to investigate the dependence of TTFs on these parameters. The results of the model agree with the existence of Blech's length, moreover, they predict the existence of a scaling relation between the MTF and the line length. Finally, we have considered resistance saturation effects. In this case we have studied the properties of the resistance fluctuations, by focusing on the non-Gaussianity of the distribution and on their power spectrum. The flexibility of the theoretical approach offers a further possibility to describe and interpret phenomena which at present have not been considered. We finally emphasize that EM, which occurs in granular materials, in the presence of a significant disorder, driven by an external bias and contrasted by the growth of a mechanical stress gradient, represents a paradigmatic example of the failure process in a disordered system. Therefore, the ability of our approach to account for a wide scenario of the EM related phenomenology should be of interest in the more extensive perspective of understanding nonequilibrium and failure phenomena in disordered systems.

ACKNOWLEDGMENTS

This work has been performed within the STATE project of the INFM. Support from the cofin-03 project "Modelli e misure di rumore in nanostrutture" financed by Italian MIUR and from SPOT-NOSED Project No. IST-2001-38899 of EC is also gratefully acknowledged.

*Corresponding author's electronic address: cecilia.pennetta@unile.it

[1] M. Ohring, *Reliability and Failure of Electronic Materials and Devices* (Academic Press, San Diego, 1998).

[2] A. Scorzoni, B. Neri, C. Caprile, and F. Fantini, Mater. Sci. Rep. **7**, 143 (1991); F. Fantini, J. R. Lloyd, I. De Munari, and A. Scorzoni, Microelectron. Eng. **40**, 207 (1998).

[3] M. A. Alam, R. K. Smith, B. E. Weir, P. J. Silverman, Nature (London) **420**, 378 (2002); *Materials, Technology and Reliability for Advanced Interconnects and Low-k Dielectrics*, edited by

K. Maex, Y. C. Joo, G. S. Oehrlein, S. Ogawa, J. T. Wetzel, Mater. Res. Soc. Symp. Proc., (2000), Vol. 612.
[4] J. Cho, C. V. Thompson, Appl. Phys. Lett. **54**, 2577 (1989).
[5] Z. Li, C. L. Bauer, S. Mahajan, and A. G. Milnes, J. Appl. Phys. **72**, 1821 (1992); S. Ohfuji and M. Tsukada, *ibid.* **78**, 3769 (1995); N. Stojadinovic, I. Manic, S. Djoric-Veljkovic, V. Davidovic, D. Dankovic, S. Golubovic, and S. Dimitrijev, Microelectron. Reliab. **42**, 1465 (1999).
[6] R. H. Koch, Phys. Rev. B **48**, 12 217 (1993); K. Dagge, W. Frank, A. Seeger, and H. Stoll, Appl. Phys. Lett. **68**, 1198 (1996); A. M. Yassine and C. T. M. Chen, IEEE Trans. Electron Devices **44**, 180 (1997).
[7] R. G. Filippi, G. A. Biery, and R. A. Wachnik, J. Appl. Phys. **78**, 3756 (1995).
[8] R. G. Filippi, G. A. Biery, and R. A. Wachnik, Appl. Phys. Lett. **66**, 1897 (1995).
[9] R. G. Filippi, R. A. Wachnik, H. Aochi, J. R. Loyd, and M. A. Korhonen, Appl. Phys. Lett. **69**, 2350 (1996); R. G. Filippi, R. A. Wachnik, C. P. Eng, D. Chidambarrao, P. C. Wang, J. F. White, M. A. Korhonen, T. M. Shaw, R. Rosenberg, and T. D. Sullivan, J. Appl. Phys. **91**, 5787 (2002).
[10] A. Scorzoni, I. De Munari, H. Stulens, and V. D'Haeger, J. Appl. Phys. **80**, 143 (1996).
[11] A. Scorzoni, I. De Munari, R. Balboni, F. Tamarri, A. Garulli, and F. Fantini, Microelectron. Reliab. **36**, 1691 (1996).
[12] S. Foley, A. Scorzoni, R. Balboni, M. Impronta, I. De Munari, A. Mathewson, and F. Fantini, Microelectron. Reliab. **38**, 1021 (1998); A. Scorzoni, S. Franceschini, R. Balboni, M. Impronta, I. De Munari, and F. Fantini, *ibid.* **37**, 1479 (1997).
[13] J. Guo, B. K. Jones, and G. Trefán, Microelectron. Reliab. **39**, 1677 (1999); V. Dattilo, B. Neri, and C. Ciofi, *ibid.* **40**, 1323 (2000).
[14] M. Gall, C. Capasso, D. Jawarani, R. Hernandez, H. Kawasaki, and P. S. Ho, J. Appl. Phys. **90**, 732 (2001); Appl. Phys. Lett. **76**, 843 (2000).
[15] J. S. Huang, T. L. Shofner, and J. Zhao, J. Appl. Phys. **89**, 2130 (2001); G. Schneider, D. Hambach, B. Niemann, B. Kaulich, J. Susini, N. Hoffmann, and W. Hasse, Appl. Phys. Lett. **78**, 1936 (2001).
[16] B. C. Valek, J. C. Bravman, N. Tamura, A. A. MacDowell, R. S. Celestre, H. A. Padmore, R. Spolenak, W. L. Brown, B. W. Batterman, and J. R. Patel, Appl. Phys. Lett. **81**, 4168 (2002).
[17] M. Shatzkes and J. R. Lloyd, J. Appl. Phys. **59**, 3980 (1986).
[18] J. R. Lloyd and J. Kitchin, J. Appl. Phys. **69**, 2117, 1991.
[19] M. A. Korhonen, P. Borgesen, D. D. Brown, and C. Y. Li, J. Appl. Phys. **74**, 4995 (1993); M. A. Korhonen, P. Borgesen, K. N. Tu, and C. Y. Li, *ibid.* **73**, 3790 (1993).
[20] R. M. Bradley and K. Wu, Phys. Rev. E **50**, R631 (1994); K. Wu and R. M. Bradley, Phys. Rev. B **50**, 12 468 (1994); K. M. Crosby and R. M. Bradley, *ibid.* **56**, 8743 (1997); R. M. Bradley, M. Mahadevan, and K. Wu, Philos. Mag. B **79**, 257 (1999).
[21] B. D. Knowlton, J. J. Clement, and C. V. Thompson, J. Appl. Phys. **81**, 6073 (1997); J. J. Clement, *ibid.* **82**, 5991 (1997); B. D. Knowlton and C. V. Thompson, J. Mater. Res. **13**, 1164 (1998).
[22] M. Schimschak and J. Krug, Phys. Rev. Lett. **80**, 1674 (1998); M. R. Gungor and D. Maroudas, Appl. Phys. Lett. **72**, 3452 (1998).
[23] M. Tammaro and B. Setlik, J. Appl. Phys. **85**, 7127 (1999); A. S. Oates, Appl. Phys. Lett. **66**, 1475 (1995).
[24] S. A. Chizhik, A. A. Matvienko, A. A. Sidelnikov, and J. Proost, J. Appl. Phys. **88**, 3301 (2000).
[25] K. Sasagawa, M. Hasegawa, M. Saka, and H. Abé, J. Appl. Phys. **91**, 1882 (2002).
[26] J. R. Black, in *Proceedings of 5th IEEE International Reliability Physics Symposium* 1967, p. 148.
[27] I. A. Blech, J. Appl. Phys. **47**, 1203 (1976); I. A. Blech and C. Herring, Appl. Phys. Lett. **29**, 132 (1976).
[28] C. Pennetta, L. Reggiani, G. Trefán, F. Fantini, A. Scorzoni, and I. De Munari, J. Phys. D **34**, 1421 (2001); C. Pennetta, L. Reggiani, G. Trefan, F. Fantini, A. Scorzoni, and I. De Munari, Comput. Mater. Sci. **22**, 13 (2001).
[29] J. P. Dekker, C. A. Volkert, E. Arzt, and P. Gumbsch, Phys. Rev. Lett. **87**, 035901 (2001).
[30] H. K. Kao, G. S. Cargill, and C. K. Hu, J. Appl. Phys. **89**, 2588 (2001).
[31] B. K. Chakrabarti and L. Benguigui, *Statistical Physics of Fracture and Breakdown in Disordered Systems* (Oxford University Press, Oxford, 1997); H. J. Herrmann and S. Roux, *Statistical Models for the Fracture of Disordered Media* (North-Holland, Amsterdam, 1990).
[32] D. Stauffer and A. Aharony, *Introduction to Percolation Theory* (Taylor and Francis, London, 1992).
[33] M. Sahimi, Phys. Rep. **306**, 213 (1998).
[34] S. Torquato, *Random Heterogeneous Materials, Microscopic and Macroscopic Properties* (Springer-Verlag, New York, 2002).
[35] L. De Arcangelis, S. Redner, and H. J. Herrmann, J. Phys. (France) Lett. **46**, 585 (1985); L. De Arcangelis, A. Hansen, H. J. Herrmann, and S. Roux, Phys. Rev. B **40**, 877 (1989).
[36] Z. Gingl, C. Pennetta, L. B. Kiss, and L. Reggiani, Semicond. Sci. Technol. **11**, 1770 (1996).
[37] C. Pennetta, L. Reggiani, and G. Trefán, Phys. Rev. Lett. **84**, 5006 (2000); C. Pennetta, L. Reggiani, and L. B. Kish, Physica A **266**, 214 (1999).
[38] C. Pennetta, L. Reggiani, and E. Alfinito, Math. Comput. Simul. **62**, 495 (2003).
[39] M. Lavine, Science **303**, 314 (2004).
[40] M. E. Eberhart, *Why Things Break, Understanding the World by the Way It Comes Apart* (Harmony Books, New York, 2003).
[41] C. D. Mukherjee, K. K. Bardhan, and M. B. Heaney, Phys. Rev. Lett. **83**, 1215 (1999); C. D. Mukherjee and K. K. Bardhan, *ibid.* **91**, 025702 (2003).
[42] A. Politi, S. Ciliberto, and R. Scorretti, Phys. Rev. E **66**, 026107 (2002).
[43] J. V. Andersen, D. Sornette, and K. T. Leung, Phys. Rev. Lett. **78**, 2140 (1997); L. Lamaignère, F. Carmona, and D. Sornette, *ibid.* **77**, 2738 (1996).
[44] S. Zapperi, P. Ray, H. E. Stanley, and A. Vespignani, Phys. Rev. Lett. **78**, 1408 (1997).
[45] A. Hansen, S. Roux, and E. L. Hinrichsen, Europhys. Lett. **13**, 517 (1990); Y. Yagil, G. Deutscher, and D. J. Bergman, Phys. Rev. Lett. **69**, 1423 (1992).
[46] D. Sornette and C. Vanneste, Phys. Rev. Lett. **68**, 612 (1992); C. Vanneste and D. Sornette, J. Phys. I **2**, 16212 (1992).
[47] Time dependent effects on the heat diffusion have been studied by D. Sornette and C. Vanneste in Ref. 46. In fact, Eq. (4) can be obtained from the expression used by Sornette *et al.* by assuming an instantaneous thermalization of each resistor and by adding the contribution of the power dissipated on first neighbor resistors.
[48] The resistance R_{perf} of a perfect network made by elementary resistors of resistance r is given by the following expression: $R_{perf}=rN_L/(N_W+1)$.

[49] C. Pennetta, L. Reggiani, G. Trefán, E. Alfinito, Phys. Rev. E **65**, 066119 (2002); C. Pennetta, Fluct. Noise Lett. **2**, R29 (2002).

[50] C. Pennetta, G. Trefán, and L. Reggiani, in *Unsolved Problems of Noise and Fluctuations*, AIP Conf. Proc. 551, edited by D. Abbott and L. B. Kish, (American Institute of Physics, Melville, NY, 1999).

[51] In a lognormal plot, the stochastic variable (the failure time in this case) is represented on a logarithmic scale while a suitable transformation is applied to the coordinates of the axis representing the cumulative distribution function in such a manner that a lognormal distribution appears as a straight line. This kind of representation is thus particularly helpful to evaluate the lognormality of a distribution and, for this reason, it is usually adopted in reliability analysis. Further details can be found in Ref. 1.

[52] C. Pennetta, G. Trefán, and L. Reggiani, Phys. Rev. Lett. **85**, 5238 (2000).

[53] K. Sieradzki, K. Bailey, and T. L. Alford, Appl. Phys. Lett. **79**, 3401 (2001); H. C. Kim, T. L. Alford, and D. R. Allee, *ibid.* **81**, 4287 (2002).

[54] This quantity, defined as the arithmetical average of TTFs is different from t_{50} although its value is close to that of t_{50}.

[55] R. M. Ziff, Phys. Rev. Lett. **69**, 2670 (1992).

[56] C. Pennetta, L. Reggiani, and G. Trefán, Math. Comput. Simul. **55**, 231 (2001).

[57] In our approach a thin line is described as a two-dimensional network, thus the current density must be associated with quantity I/N_W.

[58] M. B. Weissman, Rev. Mod. Phys. **60**, 537 (1988).

[59] N. Vandewalle, M. Ausloos, M. Houssa, P. W. Mertens, and M. M. Heyns, Appl. Phys. Lett. **74**, 1579 (1999); I. Bloom and I. Balberg, *ibid.* **74**, 1427 (1999).

[60] S. T. Bramwell, K. Christensen, J. Y. Fortin, P. C. W. Holdsworth, H. J. Jensen, S. Lise, J. M. Lopez, M. Nicodemi, J. F. Pinton, and M. Sellitto, Phys. Rev. Lett. **84**, 3744 (2000); S.T. Bramwell, P.C.W. Holdsworth, and J. F. Pinton, Nature (London) **396**, 552 (1998).

[61] C. Pennetta, E. Alfinito, L. Reggiani, and S. Ruffo, Semicond. Sci. Technol. **19**, S164 (2004); C. Pennetta, E. Alfinito, L. Reggiani, and S. Ruffo, Physica A **340**, 380 (2004).